Temperature time-history measurements in a shock tube using diode laser absorption of CO_2 near 2.7 μm

Wei Ren, Sijie Li, David F Davidson, and Ronald K Hanson
High Temperature Gasdynamics Laboratory, Department of Mechanical Engineering
Stanford, CA 94305, US

1 Introduction

Shock tubes can be used to study chemical kinetics at elevated temperatures as they provide a well-controlled pressure and temperature environment [1]. The initial temperature (T_5) and pressure (P_5) behind reflected shock waves can be routinely inferred from the measured incident shock velocity by using the traditional shock equations. However, non-ideal effects such as incident shock attenuation and boundary layer growth, disturb flow uniformities resulting in time- and space-varying temperature and pressure behind the reflected shock wave. These changes can be predicted using Mirels' boundary layer theory [2, 3]. When performing chemistry studies in a shock tube, this variation in reaction temperature can cause large uncertainties in the measurements of rate coefficients and ignition delay times [4].

In this work, a temperature sensor with 40 kHz bandwidth based on wavelength-modulation absorption spectroscopy of CO_2 was applied to investigate the temperature time-histories behind both incident and reflected shock waves. The sensor accuracy was first demonstrated by measuring the initial temperature (1100-1500 K) of CO_2/Ar behind reflected shock waves at a location 2 cm from the shock tube endwall. Temperature time-histories behind incident shock waves (640-850 K) and reflected shock waves were then measured at a second location 69.3 cm from the endwall. Repeatable experimental results reveal the fact that the temperature in region 2 declines slightly before increasing with time, which is not predicted by Mirels' model. However, an extended Mirels' model including the effect of the laminar-turbulent boundary layer transition, recently developed in our laboratory [5], can well explain this observation. We expect this gasdynamic model can be used to further extend our knowledge of the shock tube performance.

2 Sensor description and experimental setup

Tunable diode laser (TDL) absorption sensors have been widely used to provide fast, non-intrusive and *in situ* measurements of multiple gaseous parameters, such as temperature, pressure, species concentration, and velocity [6]. CO_2 is a particularly attractive target species since it is a primary combustion product of hydrocarbon fuels and can be added as an inert tracer for the measurements in both non-reactive and many reactive flow environments. The absorption spectrum of CO_2 in the $\nu_1+\nu_3$ combination band near 2.7 μm was systematically analyzed to select the optimal line pair for the TDL temperature sensor under the conditions studied [7]. The stronger absorption (approximately 1000 and 50 times stronger compared to the combination bands near 1.57 μm and 2.0 μm) and well-separated

Correspondence to: renwei@stanford.edu

values of lower-state-energy (*E''*) enable higher species detectivity and temperature sensitivity in the temperature range of 500-1600 K. Wavelength-modulation spectroscopy with 1f-normalized second-harmonic detection (WMS-2f/1f) was applied to improve the SNR for small amount of absorption and to exclude various noises due to beam steering, window fouling, and radiative emission during shock tube experiments. Additional details about the sensor design and fundamentals of wavelength-modulation spectroscopy can be found in [7, 8].

All experiments were performed in a pressure-driven shock tube with 14.1 cm inner-diameter; see reference [9] for further details about this shock tube. The incident shock wave propagates through the tube, raising the temperature and pressure of the test gas from (T_1, P_1) to (T_2, P_2); when it encounters the endwall of the tube, the shock wave is reflected and further elevates the test gas properties to (T_5, P_5). The gas temperature and pressure immediately behind the shock wave can be accurately calculated using standard normal-shock relations and the measured incident shock speed [1].

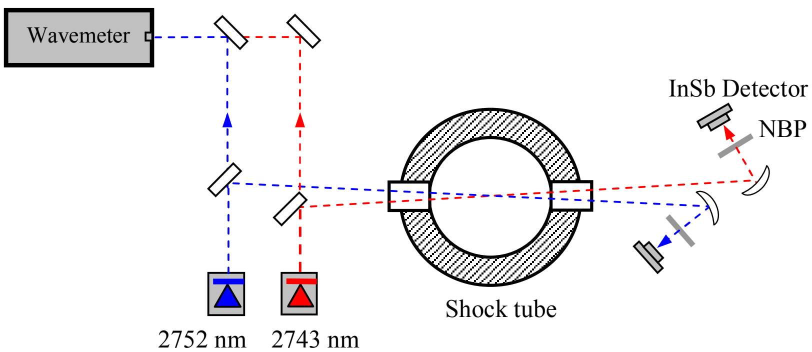

Figure 1. Shock tube experimental setup. Wavemeter: Bristol model 621, used to verify the center wavelength without modulation; NBP: narrow bandpass filter.

A schematic of the experimental setup for two-wavelength absorption measurement in the shock tube is shown in Figure 1. Two continuous-wavelength (cw) distributed-feedback (DFB) diode lasers from NanoPlus were sinusoidally modulated by 100 kHz digital waveforms with optimized modulation depths [8], for the selected transitions R28 near 2752 nm and P70 near 2743 nm. On the collection side the collimated beam from each laser was focused onto a liquid-nitrogen-cooled InSb detector (IR Associates IS-2.0). The detector signals were sampled at a rate of 10 MHz and demodulated by a digital lock-in amplifier on LabVIEW with a low-pass filter bandwidth of 40 kHz to extract the 1f and 2f signals. Gas temperature can be obtained from the measured ratio of the 1f-normalized WMS-2f signal near the line-center of the two selected transitions [8]. During shock tube measurements, the sensor accuracy was first demonstrated by measuring reflected shock temperatures (1100-1500 K) of non-reactive CO_2/Ar gas mixture at 2 cm from the shock tube endwall. The second test location was then established upstream (69.3 cm from the endwall) to clearly observe the temperature variation with time behind the incident shock wave.

3 Experimental results

The initial gas temperature and pressure behind the reflected shock can be accurately calculated, assuming vibrational equilibrium and frozen chemistry. The laser diagnostic was located 2 cm from the shock tube endwall. A typical temperature time-history of 2% CO_2/Ar behind the reflected shock is shown in Figure 2 along with the corresponding pressure trace recorded using a Kistler piezo-electric transducer. The average measured temperature over the initial time interval 0.1-0.5 ms was 1193 K with a standard deviation of ~5 K, which was in excellent agreement with the expected value of 1199 K calculated using normal-shock relations. The sensor successfully captured the slight rise of temperature (beginning at ~0.6 ms, with $\Delta T/\Delta t$ = +2.1%/ms) attributed to the effects of boundary layer growth and shock attenuation, which will be further discussed in the following section. In addition, the temperature profile calculated using isentropic compression ($\gamma_{mixture} = 1.654$) is also plotted in Figure 2 for comparison, verifying the fact that the post-shock temperature follows the pressure isentropically.

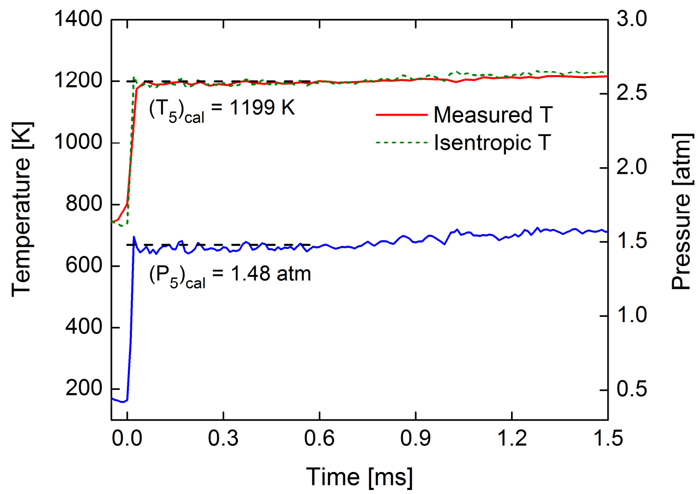

Figure 2. Measured temperature and pressure time-histories at 2 cm from shock tube endwall. Initial conditions: 2% CO_2/Ar, P_1 = 55.0 Torr, T_1 = 298 K; incident shock conditions (calculated): P_2 = 0.43 atm, T_2 = 697 K; reflected shock conditions (calculated): P_5 = 1.48 atm, T_5 = 1199 K.

Additional experiments were conducted under different shock conditions shown in Figure 3 (square points), comparing the measured temperatures (averaged over the initial time interval 0.1-0.5 ms) with the expected values. These comparisons demonstrate a good agreement between measurements and simulations (within 1.5%) over the entire temperature range of 1100-1500 K.

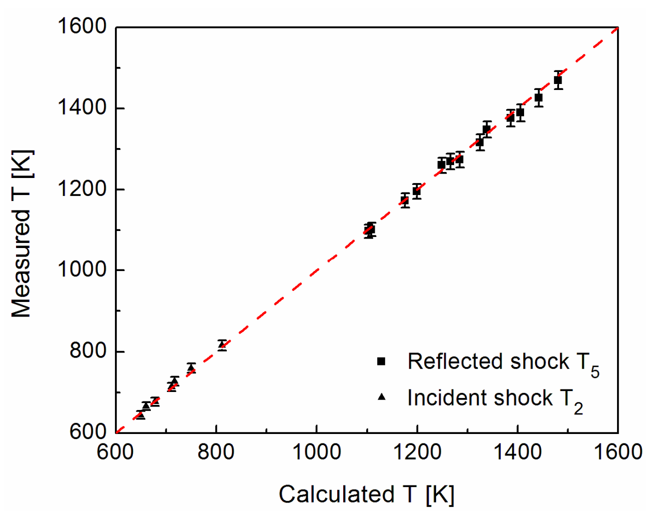

Figure 3. Temperatures measured using the WMS-2f sensor versus calculated values using the shock jump equations; ±1.5% error bars. Square points: T_5 behind reflected shock waves (P_5 = 1.0-1.5 atm); triangular points: T_2 behind incident shock waves (P_2 = 0.4-0.6 atm).

After the sensor was validated at the location 2 cm from the endwall, a second test location was established 69.3 cm from the endwall to investigate the temperature time-histories behind both incident and reflected shocks. Since the initial temperature in region 2 (T_2) can be accurately calculated using measured shock speed, the measured T_2 was also compared with calculations as illustrated in Figure 3 (triangular points). Good agreement can be seen between the measured and the calculated temperatures, within 1.5% over the full 640-1500 K range. Figure 4 demonstrates a typical temperature and pressure time-histories at 69.3 cm from the endwall with 2% CO_2/Ar mixture initially at P_1 = 50 Torr, T_1 = 298 K. These time-histories reveal the fact that the temperature and pressure behind the incident shock remains almost constant (though it does decline slightly in the first 1.2 ms) before the arrival of the reflected shock, which is not the case predicted by Mirels' theory as shown in Figure 5. The Mirels' model over-estimates the temperature rise with time behind both the incident and reflected shock waves.

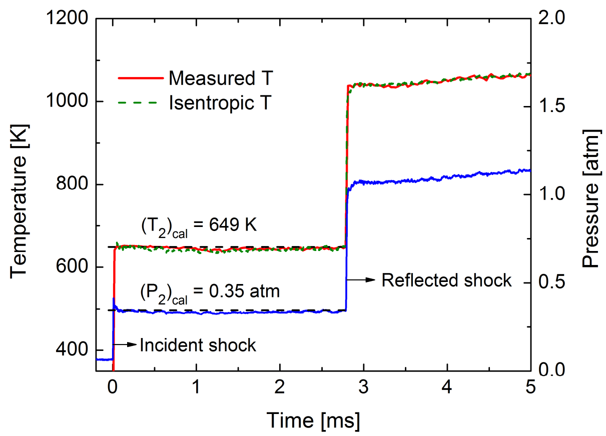

Figure 4. Measured temperature and pressure time-histories at 69.3 cm from the endwall with 2% CO_2/argon mixture. Initial: P_1 = 50.1 Torr, T_1 = 298 K; incident shock (calculated): P_2 = 0.35 atm, T_2 = 649 K.

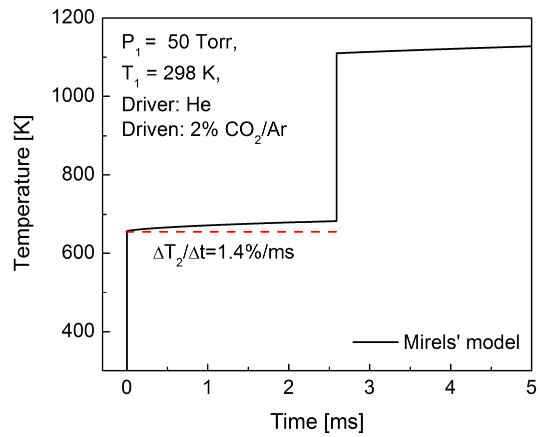

Figure 5. Simulated temperature time-history using Mirels' theory by assuming completely turbulent boundary layer.

4 Discussion

In Mirels' model, the boundary layer was assumed either completely laminar or turbulent. In real cases, however, a laminar boundary layer exists before transition to the turbulent boundary layer, which is determined by a transition Reynolds number [10]. Thus the extended model should more accurately account for the actual post-shock wave conditions by including the turbulent-laminar boundary layer transition [11]. In the current version of the Mirels' gasdynamic model developed in our laboratory [5], Rudinger's method [12] was implemented to calculate time- and space-varying flow variables in region 5. To simplify calculations, the boundary layer transition length, the gas velocity in region 5, and the entropy changes along characteristic lines were neglected. The boundary layer effect was averaged over the tube cross-section and eqivalent to 1-D study.

A laminar boundary layer is first formed behind the incident shock front and this boundary layer affects the conditions at the observation test location. As the shock wave propagates, the region of the laminar boundary layer that affects the test location reduces with time until the transition point arrives. Simultaneously, an increasing portion of turbulent boundary layer that has bigger mass sink effects than laminar boundary layer also starts to affect the test location. The net mass sink effect thus causes the temperature to decline first. Since the laminar part is relatively short, the temperature behind the incident shock decreases only to a small extent. After the passing by of transition point, only the turbulent boundary layer affects the test location and the temperature begins to rise as expected by Mirels' model. Therefore, the competition between laminar and turbulent layers plays an essential role in determining the temperature (and also other flow properties) non-uniformity in region 2.

Figure 6 compares the simulated temperature time-history including the effect of the boundary layer transition, to the experimental results for the same shock tube experiment as shown in Figure 4. Notice that the transition Reynolds number (0-10^6) was optimized to achieve a good agreement with the measurement. At the test location 69.3 cm from the endwall, the simulated results using the extended Mirels' model predicted a slight decrease of temperature before increasing back, which is exactly the case seen in the experiment.

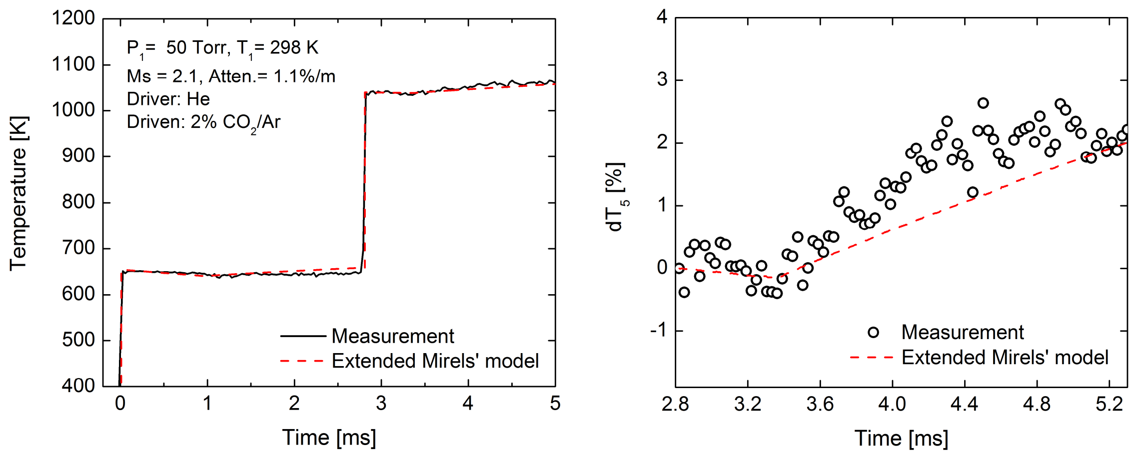

(a) Temperature variation in region 2 and region 5. (b) Percentage temperature variation in region 5.

Figure 6. Measured and simulated temperature time-histories at 69.3 cm from the endwall (the same shock conditions as described in Figure 4); a transition Reynolds number of 8×10^5 used in the simulation.

When the shock wave is reflected by the endwall, the flow properties immediately behind the shock wave are determined by the upstream conditions in region 2 and the inferred reflected shock strength. The flow conditions at other region 5 locations (here 69.3 cm from the endwall) are related to the points behind the reflected shock through characteristic lines. The influence of the non-uniformities in region 2 will be amplified by the reflected shock: T_5 initially decreases slightly and then increases continuously. Since the transition region is very short, the slight temperature decline appears almost flat in Figure 6(a). Figure 6(b) compares the measured and simulated percentage T_5 change versus time, showing good agreement with each other. Notice that the vibrational relaxation in the lower energy levels of CO_2 occurs rapidly behind these shock waves in CO_2/Ar mixtures; in fact, measured vibrational relaxation time under our experimental conditions was shown to be less than 20 μs [13].

5 Conclusions

A TDL absorption sensor based on the WMS-2f/1f technique was used for rapid and sensitive temperature measurement of CO_2 in a shock tube. Excellent agreement (within 1.5%) was found between the measured initial temperatures (incident shock: 640-850 K, reflected shock: 1100-1500 K) and the calculated values using shock jump equations. Non-uniformities in the temperature time-histories were observed behind both incident and reflected shocks. The measured temperature declined slightly first before increasing with time, which was not predicted by the Mirels' boundary layer theory. By including the effect of the turbulent-laminar boundary layer transition, the Mirels' model was extended to better predict the flow conditions behind shock waves.

6 Acknowledgements

This work was supported by the Air Force Office of Scientific Research.

References

[1] Hanson RK, Davidson DF. (2001). Handbook of shock waves. 1: Chap. 5.2. Academic Press, San Diego.
[2] Mirels H, Mullen JF. (1964). Small perturbation theory for shock tube attenuation and non-uniformity. Phys .Fluids. 7: 1208.
[3] Mirels H. (1972). Boundary layer growth effects in shock tubes. Proc. 8th Int. Comb. Symp.: BJ62.
[4] Bowman CT, Hanson RK. (1979). Shock tube measurements of rate coefficients of elementary gas reactions. J. Phys. Chem. 83: 757.
[5] Li S, Ren W, Davidson DF, Hanson RK. (2011). Flow non-uniformity behind incident and reflected shock waves due to boundary layer formation in a shock tube. Submitted to ISSW 28th, Manchester, UK.
[6] Hanson RK. (2011). Applications of quantitative laser sensors to kinetics, propulsion and practical energy systems. Proc. Combust. Inst. 33: 1.
[7] Farooq A, Jeffries JB and Hanson RK. (2008). CO_2 concentration and temperature sensor for combustion gases using diode-laser absorption near 2.7 μm. Appl. Phys. B 90: 619.
[8] Li H et al. (2006). Extension of wavelength-modulation spectroscopy to large modulation depth for diode laser absorption measurements in high-pressure gases. Appl. Opt. 45: 1052.
[9] Oehlschlaeger MA, Davidson DF and Hanson RK. (2004). High-Temperature thermal decomposition of isobutane and *n*-butane behind shock waves. J. Phys. Chem. A. 108: 4247.
[10] Hartunian RA, Russo AL, Marrone PV. (1960). Boundary layer transition and heat transfer in shock tubes. J. Aerospace Sci. 27: 587.
[11] Petersen EL. (1998). A shock tube and diagnostics for chemistry measurements at elevated pressures with application to methane ignition. Ph.D. diss., Stanford University.
[12] Rudinger G. (1961). Effect of boundary-layer growth in a shock tube on shock reflection from a closed end. Phys. of Fluids, 4:1463.
[13] Simpson CJSM, Chandler TRD and Strawson AC. (1969). Vibrational relaxation in CO_2 and CO_2-Ar mixtures studied using a shock tube and a laser–schlieren technique. J. Chem. Phys. 51: 2214